NIH Public Access
Author Manuscript
Int J Comput Assist Radiol Surg. Author manuscript; available in PMC 2011 June 14.

Published in final edited form as:
Int J Comput Assist Radiol Surg. 2010 May ; 5(3): 221–228. doi:10.1007/s11548-009-0391-1.

Effect of brain shift on the creation of functional atlases for deep brain stimulation surgery

Srivatsan Pallavaram,
Department of Electrical Engineering, Vanderbilt University, VU Station B 351662, Nashville, TN 37240-1662, USA

Benoit M. Dawant,
Department of Electrical Engineering, Vanderbilt University, VU Station B 351662, Nashville, TN 37240-1662, USA

Michael S. Remple,
Department of Neurosurgery, Vanderbilt Medical Center, Nashville, TN, USA

Joseph S. Neimat,
Department of Neurosurgery, Vanderbilt Medical Center, Nashville, TN, USA

Chris Kao,
Department of Neurosurgery, Vanderbilt Medical Center, Nashville, TN, USA

Peter E. Konrad, and
Department of Neurosurgery, Vanderbilt Medical Center, Nashville, TN, USA

Pierre-François D'Haese
Department of Electrical Engineering, Vanderbilt University, VU Station B 351662, Nashville, TN 37240-1662, USA

Srivatsan Pallavaram: sri.pallavaram@vanderbilt.edu; Benoit M. Dawant: benoit.dawant@vanderbilt.edu

Abstract

Purpose—In the recent past many groups have tried to build functional atlases of the deep brain using intra-operatively acquired information such as stimulation responses or micro-electrode recordings. An underlying assumption in building such atlases is that anatomical structures do not move between pre-operative imaging and intra-operative recording. In this study, we present evidences that this assumption is not valid. We quantify the effect of brain shift between pre-operative imaging and intra-operative recording on the creation of functional atlases using intra-operative somatotopy recordings and stimulation response data.

Methods—A total of 73 somatotopy points from 24 bilateral subthalamic nucleus (STN) implantations and 52 eye deviation stimulation response points from 17 bilateral STN implantations were used. These points were spatially normalized on a magnetic resonance imaging (MRI) atlas using a fully automatic non-rigid registration algorithm. Each implantation was categorized as having *low*, *medium* or *large* brain shift based on the amount of pneumocephalus visible on post-operative CT. The locations of somatotopy clusters and stimulation maps were analyzed for each category.

Results—The centroid of the *large* brain shift cluster of the somatotopy data (posterior, lateral, inferior: 3.06, 11.27, 5.36 mm) was found posterior, medial and inferior to that of the *medium*

© CARS 2009

Correspondence to: Benoit M. Dawant, benoit.dawant@vanderbilt.edu.

NIH-PA Author Manuscript
NIH-PA Author Manuscript
NIH-PA Author Manuscript

NIH-PA Author Manuscript

NIH-PA Author Manuscript

NIH-PA Author Manuscript

cluster (2.90, 13.57, 4.53 mm) which was posterior, medial and inferior to that of the *low* shift cluster (1.94, 13.92, 3.20 mm). The coordinates are referenced with respect to the mid-commissural point. Euclidean distances between the centroids were 1.68, 2.44 and 3.59 mm, respectively for *low-medium, medium-large and low-large* shift clusters. We found similar trends for the positions of the stimulation maps. The Euclidian distance between the highest probability locations on the *low* and *medium-large* shift maps was 4.06 mm.

Conclusion—The effect of brain shift in deep brain stimulation (DBS) surgery has been demonstrated using intra-operative somatotopy recordings as well as stimulation response data. The results not only indicate that considerable brain shift happens before micro-electrode recordings in DBS but also that brain shift affects the creation of accurate functional atlases. Therefore, care must be taken when building and using such atlases of intra-operative data and also when using intra-operative data to validate anatomical atlases.

Keywords

Intra-operative brain shift; Functional/statistical atlases; Deep brain stimulation

Introduction

Deep brain stimulation (DBS) is a method used to alleviate symptoms related to movement disorders such as Parkinson's disease by stimulating deep brain nuclei. Because of the small size of the nuclei, such functional neurosurgical procedures require precise targeting. Traditionally, they are performed in two stages. An approximate target location is first selected pre-operatively by a neurosurgeon and then refined intra-operatively using multiple exploratory electrodes to map the electrophysiology of the brain around the planned target. Although this process permits some compensation of brain shift and adjustment of the target, it is time consuming and requires expertise that is not always available.

Because the surgical targets of interest used for movement disorders are not or poorly visible in typical imaging modalities, a number of computerized methods have been developed to assist surgeons in planning the procedure. These typically involve the use of an atlas and its registration to the patient's MR images. The current clinical standard atlases are the Talairach [1] and the Schaltenbrand–Wahren atlas [2]. These consist of a series of unevenly spaced brain sections that have been histologically stained to reveal the structures and sub-structures of interest. When digitized, these atlases can be superimposed on the preoperative images. But these atlases are imperfect because they are either limited to one sectioning plane per hemisphere (Talairach atlas) or to non-contiguous anatomy in intersecting orthogonal slices (S-W atlas). Alternatives to these atlases have been developed recently [3–6]. These approaches involve one 3D histological atlas reconstructed from thin contiguous slices registered to one MR image volume. Automatic segmentation of structures such as the STN, substantia nigra, or red nucleus is then obtained by registering the atlas MR volume to the patient MR volume. There is, however, a lack of consensus on the exact anatomical location at which stimulation can provide the best efficacy for a given disease. For instance, it has been reported by Plaha et al. [7] that both the dorsal part of the STN and zona incerta (ZI) provide symptom relief. Maks et al. [8] have recently reported that patient-specific models showed that therapeutic benefits were achieved with direct stimulation of a wide range of anatomical structures in the STN region in 10 Parkinson's disease (PD) patients. Andrade-Souza et al. [9] use a target near the superior portion of the nucleus. Based on micro-electrode recordings (MER), Hamani et al. [10] found that STN-like activity was recorded up to 3 mm more anterior than the anterior border of the nucleus defined with the MRI; indicating that STN extended more anteriorly than suggested by MRI. There is thus

NIH-PA Author Manuscript

NIH-PA Author Manuscript

NIH-PA Author Manuscript

evidence that the anatomy can only be used as a guide and that electrophysiological atlases may provide more useful information.

The concept used in electrophysiological atlases is similar to the concept used in anatomical atlases: first build an atlas, and then use this atlas for targeting. The atlas creation step is, however, different. Typically, the final intra-operative position of the lead, the intra-operative response to stimulation at specific points, intra-operative micro-electrode recordings, and the position of the active contact in post-operative images are gathered for a population in image coordinates. This information is then spatially normalized by registering individual image volumes to one or several reference image volumes, and statistical atlases are created. This is the approach followed by Tasker et al. [11], Finnis et al. [12,13], Nowinsky et al. [14–16], Guo et al. [17,18], Toga et al. [19], Castro et al. [20,21], and ourselves [22–25]. In [26], Guo et al. compared a number of methods for STN DBS targeting including direct targeting, use of anatomical atlases, electrophysiological databases, actual surgical targets from a population of patients, and a combination of these methods. They found that the electrophysiological atlas, actual surgical target collection, and the combination of approaches based on functional and anatomical information provided more accurate initial estimation of the surgical target positions than those techniques dependent solely on anatomical references.

But, an underlying assumption commonly used when building physiological atlases is that anatomical structures do not move between pre-operative imaging and intra-operative recording. This assumption is made even though a number of studies have shown the occurrence of brain shift in stereotactic surgery [27–32]. In 1975, Gerdes et al. [27] first described the error resulting from subdural air invasion and “brain sinking” in a stereotactic procedure. Similarly, Khan et al. [31] analyzed brain shift between pre-operative and post-operative 3D MRI scans in 25 subjects. They reported brain shifts of up to 4 mm in magnitude and mostly observed in the direction of gravity, with deeper structures experiencing smaller shift than more superficial structures. Miyagi et al. [30] investigated the tendency, direction, and extent of brain shift by comparing the locations of anterior and posterior commissures (AC and PC) on the pre- and post-operative MRI. Both the commissures were found more medial, posterior and inferior on the post-operative MRI than on the pre-operative MRI. In a 2008 study, Halpern et al. [32] reported shift impacted the number of microelectrode tracks needed to optimize targeting.

Because of shift, stereotactic coordinates of intra-operative data may be different from their anatomical locations. This can, in turn, impact the accuracy of electrophysiological atlases created with this data. In this study, we evaluate this effect using somatotopy recordings and stimulation response data and demonstrate that intra-operative brain shift can have a substantial effect on the resulting statistical maps.

Data

Image data

With IRB approval each patient had pre-operative MRI and CT, and a post-operative CT acquired on the day of the surgery, which will be referred to as the post-op CT. Typical CT images were acquired at kVp = 120 V, exposure 350 mAs and 512 × 512 pixels. In-plane resolution and slice thickness were approximately 0.5 and 0.75 mm, respectively. MRI (TR 12.2 ms, TE 2.4 ms, 256 × 256 × 170 voxels, with typical voxel resolution of 1 × 1 × 1 mm^3) were acquired using the SENSE parallel imaging technique (T1W/3D/TFE) from Philips on a 3 T scanner.

NIH-PA Author Manuscript

NIH-PA Author Manuscript

NIH-PA Author Manuscript

At our institution the surgery is performed with a miniature stereotactic frame, the StarFix microTargeting Platform® (501(K), Number K003776, Feb. 23, 2001, FHC, INC; Bowdoin, ME) instead of a standard stereotactic frame. During surgery, a micro-positioning drive (microTargeting® drive system, FHC Inc., Bowdoin, ME) is mounted on the platform. Recording and stimulating leads are then inserted through the guiding tubes. Details on the platform, including a study of its accuracy demonstrating it to be at least as accurate as standard frames can be found in [33,34].

Somatotopy and stimulation response data

Intra-operative somatotopy and stimulation responses were recorded for this study. A somatotopic response is said to be observed at a given location in the brain when a noticeable change in micro-electrode recordings follows a stimulus such as flexion or extension of body parts such as elbow, shoulder or wrist. Only those observations recorded with confidence as determined by the surgical team were used. A total of 24 bilateral sub-thalamic nucleus (STN) implantations contributing 73 somatotopy data points were used.

Eye deviation responses to stimulation were also used to create functional atlases. A total of 52 data points from 17 bilateral STN implantations were utilized. Although other types of response to stimulation were available, we have chosen to limit this study to eye deviation data because it is the most populous stimulation response dataset we have.

Method

Registration and data pre-processing

A key component of the method is our ability to map information acquired from a population of patients onto one reference image volume, termed the atlas. This has been demonstrated in our earlier works [22,23,25,35]. Two types of registration algorithms are needed to perform such mapping; rigid and non-rigid. The rigid registration algorithm is required to align pre-operative MRI and CT (CT scans are acquired at our institution because the stereotactic frame we use—see “Image data”—requires it) scans of the same patient. Non-rigid registration is required to map patient data onto the atlas. In this study, non-rigid registration is always performed on MRI volumes using the adaptive bases algorithm we have proposed earlier [36]. Briefly, this algorithm computes a deformation field that is modeled as a linear combination of radial basis functions with finite support. This results in a transformation with several thousands of degrees of freedom. Two transformations (one from the atlas to the subject and the other from the subject to the atlas) that are constrained to be inverses of each other are computed simultaneously. The adaptive bases algorithm reduces the computational complexity and improves the convergence properties of related B-splines-based approaches by identifying regions of mis-registration and adapting the compliance of the transformation locally. The algorithm arrives at the final deformation iteratively across scales and resolutions. The similarity measure used by both algorithms is the mutual information between the images [37,38], which is commonly used for medical image registration tasks (see Pluim et al. [39] for a good review).

Classification of the data based on brain shift

In previous work [40] we showed that brain shift in the deep brain is proportional to the amount of air invasion or pneumocephalus. Shift in the deep brain was measured as the difference between the implant location on the post-op CT acquired immediately after surgery and that on the delayed CT acquired about a month after surgery when the brain is expected to have recovered from brain shift. Similarly, Halpern et al. [32] reported that AC-PC shortening correlated with cortical displacement measured based on the amount of pneumocephalus.

NIH-PA Author Manuscript

NIH-PA Author Manuscript

NIH-PA Author Manuscript

Each post-op CT was carefully inspected for pneumocephalus and each side of the brain was classified into one of the three categories: *low*, *medium* and *large* brain displacement corresponding respectively to an average air pocket width less than or equal to 3 mm, between 3 and 7 mm, and higher than 7 mm. We found negligible shift in the deep brain for air pocket width of 3 mm or less and substantial shift in the deep brain for air pocket width of 7 mm or more. The air pockets were measured from the inner table of the calvarium in the frontal cortex. Figure 1 shows representative examples of (a) *low*, (b) *medium* and (c) *large* shift patients. To determine the region in the frontal cortex where cortical surface shift is most likely to cause brain shift at the target, a reference line (shown as a dashed line in Fig. 1) parallel to the direction of gravity and passing through the implant was drawn. The measurements are made in the vicinity of this region. As shown, four measurements of the width of the air pocket were made and averaged to categorize the patient into one of the three shift groups. The direction of gravity is assumed to be along the AC–PC direction because the patients lay supine during the post-op CT acquisition. Two observers, authors SP and PFD independently made the measurements and grouped the data. Figure 1d shows a typical head orientation for a patient laying supine during the post-op CT acquisition.

Populating the atlas with intra-operative data and building stimulation maps

The depth of the electrode for every somatotopy and stimulation response data point was read from the micro-positioning device and converted into *X*, *Y*, and *Z* coordinates in pre-operative CT. The patient pre-operative MRI and CT images were registered using a rigid body registration. Each MRI volume was registered to the atlas through non-rigid registration. The transformations were concatenated and the *X*, *Y*, and *Z* coordinates of the intra-operative data were transformed into X_A, Y_A, and Z_A atlas coordinates.

The eye deviation maps were built using the method described in detail in [25]. Briefly, we assume that responsive neurons are localized somewhere on an annulus in 2D or a spherical shell in 3D centered on the stimulation point. To study a patient's response to stimulation at a given location, stimulation current is applied in steps (typically 0.5–1.0 mA) until a response is observed. If a response occurs at stimulation current I and not at the previous step $I - \varepsilon$, then we assume that the responsive neurons were activated between $I - \varepsilon$ and I where ε is a positive real number. Thus, we assume that the responsive neurons lie on this annulus or a spherical shell in 3D.We associate a uniform probability density function with the neurons in the spherical shell. Summing over a number of such stimulation points and normalizing them yields a probability map of responsive stimulation regions. Our current to radius relationship (R) is based on the data published by Butson et al. [41] for mono-polar voltage stimulation using a DBS electrode in an isotropic medium and with standard stimulator settings. Typical radius values are 2.2 mm for 1 mA, 2.6 mm for 1.5 mA, 3 mm for 2 mA. We have investigated the sensitivity of our method to the relationship between stimulation voltage/current and radius. We found that the overall size and morphology of the maps changes in their peripheral regions but that the regions of high probability were stable. At our center, stimulation is applied in steps of 0.5 mA but to account for potential delay in the occurrence of response we chose ε to be 1.

More specifically, for a data point $P_1(X_A, Y_A, Z_A)$ producing a stimulation response at I mA, a spherical shell-based stimulation map with outer radius $r_1 = R(I)$ and inner radius $r_2 = R(I - 1)$ is created as follows. Let Ω_1 be the set of all voxels inside the spherical shell (Eq. 1). The value of the map at a point with coordinates (x_A, y_A, z_A) in the image due to the observation at P_1 is $F_{P1}(x_A, y_A, z_A)$ defined in Eq. (2).

$$\Omega_1 = \left\{(x_A, y_A, z_A) \in R^3 | r_2^2 < (x_A - X_A)^2 + (y_A - Y_A)^2 + (z_A - Z_A)^2 \leq r_1^2\right\} \quad (1)$$

NIH-PA Author Manuscript

NIH-PA Author Manuscript

NIH-PA Author Manuscript

$$F_{P_1}(x_A, y_A, z_A) = \left\{ \frac{1}{n(\Omega_1)} \text{when } (x_A, y_A, z_A) \in \Omega_1, 0 \text{ otherwise} \right\} \quad (2)$$

$n(\Omega_1)$ is the number of elements in the set Ω_1

When multiple points $P_1, P_2, \ldots, P_N$ are used in building a map, the overall efficacy map F at any point (a, b, c) is defined as in Eq. (3).

$$F(a, b, c,) = \frac{1}{N} * \left(\sum_{i=1}^{N} F_{P_1}(a, b, c) \right) \quad (3)$$

The locations of somatotopy data clusters and eye deviation maps for the various brain shift groups were subsequently analyzed.

Results

Grouping data based on pneumocephalus as discussed in the section "Classification of the data based on brain shift" resulted in the following datasets. The somatotopy data was classified as eight implantations contributing 17 data points in the *low*, 12 implantations contributing 47 data points in the *medium*, and 4 implantations contributing 9 data points in the *large* air groups. For the stimulation data, the *medium* and *large* categories were merged to create the *medium-large* category because too few data points were available to build a map for the *large* category. The stimulation response data contains 25 points from 7 implantations in the *low* shift category and 27 points from 10 implantations in the *medium-large* shift category.

Transforming the coordinates of the somatotopy and stimulation response data from each of the patients onto the atlas using the registration method described in the section "Registration and data pre-processing" resulted in distinct clusters (one for each category) in the atlas. Figure 2 shows the locations of the centroids of somatotopy clusters for the *low* (red), *medium* (blue) and *large* (green) brain shift patients overlaid on the atlas MRI. Figure 2a shows the sagittal view and Fig. 2b shows the coronal view. The lateral ventricle and the interpeduncular cistern are highlighted for anatomical reference. To eliminate the effect of outliers, we also looked at the medians of the clusters and a similar organization was observed. The centroid and median were computed on each coordinate for the points in the cluster.

The locations of the centroids and medians of the clusters are given in Table 1 (in each case, the origin of the coordinate system is the mid-commissural point). Table 1a shows that the *medium* group is located posterior, inferior and medial to the *low* group and that the *large* group is posterior, inferior and medial to the *medium* group. Similar trends are observed with respect to the medians as shown in Table 1b. The standard deviations, in mm, for the posterior, lateral and inferior components of the *low*, *medium* and *large* shift groups are (2.40, 1.64, 2.01), (1.98, 1.43, 1.84) and (2.11, 1.38, 2.17) respectively. The distances between the centroids of the low and large, medium and large and low and medium clusters were 3.59, 2.44 and 1.68 mm, respectively. The distances between the medians of the low and large, medium and large and low and medium clusters were 3.36, 1.88 and 2.03 mm, respectively.

NIH-PA Author Manuscript

NIH-PA Author Manuscript

NIH-PA Author Manuscript

Figure 3 shows axial and coronal slices of the eye deviation stimulation response maps containing the highest probability point for (a) *low* and (b) *medium-large* brain shift groups overlaid on the atlas MRI. It can be seen that the shapes and locations of the maps are quite different for the two groups. The measurements in the figures indicate that the high probability region in the *medium-large* shift map is 3.5 mm medial, 1.5 mm inferior and 1.4 mm posterior to the *low* shift map resulting in a Euclidean distance of 4.06 mm between the high probability points in the two maps.

Discussion

Earlier studies have reported on brain shift by comparing locations of anatomical points (different from the target points) between pre- and post-operative images. Such studies can be affected by changes in patient posture between surgery and post-operative imaging. Their analyses can also be affected by post-implantation brain shift as well as delay between implantation and post-operative imaging. Instead, we have used intra-operative micro-electrode recording-based somatotopy observations and stimulation responses recorded from the target regions (STN for instance) to study this effect.

The distance between the centroid of the somatotopic functional atlas created using all data and that created using only the *low* brain shift data—what we think is the closest to the gold standard—is 1.46 mm. The distance between the corresponding medians is 1.74 mm. The distance between the centroids of *low* and *large* somatotopic atlases is as high as 3.59 mm. The stimulation response maps showing the region of eye deviation using *low* and *medium-large* shift data are quite different in shape and location. The distance between the high probability points on the *low* and *medium-large* maps is 4.06 mm. The *medium-large* shift map is more medial and inferior to the *low* shift map.

One potential source of error that can affect these observations is the accuracy of the registration used to map data from individual patients onto the atlas. Since the precise anatomical points corresponding to the somatotopic and stimulation response observations are not visible on current imaging, there is no direct way to evaluate the accuracy of registration at these points. However, predicting the anterior and posterior commissures which are around the typical DBS targets using the same rigid and non-rigid registration algorithms used in this paper we found the registration accuracy to be sub-millimetric [42]. Another potential source of error is the accuracy of the stereotactic system. A recent phantom study by Balachandran et al. [34] showed the accuracy of our stereotactic platform (microTargeting™ StarFix) to be 0.42 ± 0.15 mm. One of the limitations of this study is that it is dependent on cortical landmarks (air pockets at the surface of the brain) for the classification of patients into various shift groups. A more reliable approach to group patients based on shift would be to use an intra-operative CT to capture snapshots of landmarks in the vicinity of the targets at various stages of the procedure, i.e., immediately after dura opening, before micro-electrode recordings, before micro/macro stimulation and after implantation of the final electrode.

In the recent past, a number of functional atlases and databases containing intra-operatively acquired sub-cortical electrophysiological data from a number of patients have been implemented to complement anatomical and histological atlases. Several groups have used such atlases to provide targeting predictions and intra-operative guidance as discussed in the “Introduction” section. However, none of these atlases account for brain shift. A number of authors have shown the occurrence of intra-operative brain shift in DBS by comparing pre- and post-operative images. Furthermore, in a 2008 study, Halpern et al. [32] reported that shift impacted the number of microelectrode tracks needed to optimize targeting. The *DBS for PD study group* reported that the higher the number of microelectrode passes the higher

NIH-PA Author Manuscript

NIH-PA Author Manuscript

NIH-PA Author Manuscript

the risk of intracranial bleeding [43]. Therefore, intra-operative brain shift could have an impact on patient care and must be taken into account.

Our results are based on using intra-operative data to study the effect of brain shift on atlas creation. The results indicate that considerable brain shift happens before micro-electrode recordings in DBS and that brain shift should be accounted for when building functional atlases. Caution should also be used when using intra-operative recordings to validate anatomical atlases. The results in this study are not target dependent and similar results can be expected at other deep brain targets. We are now working on developing methods to compensate for brain shift when building electrophysiological atlases. This will permit using data acquired from all patients, even those for which brain shift is substantial. When these atlases are built, we will investigate their usefulness for procedure planning, intra-operative guidance, and implant programming.

Acknowledgments

This research has been supported, in parts, by NIH R01 EB006136.

References

1. Talairach, J.; Tournoux, P. Co-planar stereotaxic atlas of the human brain. New York: Thieme Publishing Group; 1988.
2. Schaltenbrand, G.; Wahren, W. New York: Thieme Publishing Group; 1977. Atlas for stereotaxy of the human brain.
3. Yelnik J, Bardinet E, Dormont D, Malandain G, Ourselin S, Tandé D, Karachi C, Ayache N, Cornu P, Agid Y. A three-dimensional, histological and deformable atlas of the human basal ganglia. I. Atlas construction based on immunohistochemical and MRI data. Neuroimage. 2007; 34:618–638. [PubMed: 17110133]
4. Bardinet E, Bhattacharjee M, Dormont D, Pidoux B, Malandain G, Schüpbach M, Ayache N, Cornu P, Agid Y, Yelnik J. A three-dimensional histological atlas of the human basal ganglia. II. Atlas deformation strategy and evaluation in deep brain stimulation for Parkinson disease. J Neurosurg. 2009; 110:208–219. [PubMed: 18976051]
5. Chakravarty MM, Bertrand G, Hodge CP, Sadikot AF, Collins DL. The creation of a brain atlas for image guided neurosurgery using serial histological data. Neuroimage. 2006; 30(2):359–376. [PubMed: 16406816]
6. Chakravarty MM, Sadikot AF, Mongia S, Bertrand G, Collins DL. Towards a multi-modal atlas for neurosurgical planning. Lecture notes in computer science (MICCAI). 2006; vol 4191:389–396.
7. Plaha P, Ben-Shlomo Y, Patel NK, Gill SS. Stimulation of the caudal zona incerta is superior to stimulation of the subthalamic nucleus in improving contralateral parkinsonism. Brain. 2006; 129:1732–1747. [PubMed: 16720681]
8. Maks CB, Butson CR, Walter BL, Vitek JL, McIntyre CC. Deep brain stimulation activation volumes and their association with neurophysiological mapping and therapeutic outcomes. Neurol Neurosurg Psychiatry. 2009 Online: 16 Jan, 2009.
9. Andrade-Souza YM, Schwalb JM, Hamani C, Eltahawy H, Hoque T, Saint-Cyr J, Lozano AM. Comparison of three methods of targeting the subthalamic nucleus for chronic stimulation in Parkinson's disease. Neurosurgery. 2008; 62(2):875–883. [PubMed: 18596420]
10. Hamani C, Richter EO, Andrade-Souza Y, Hutchison W, Saint-Cyr JA, Lozano AM. Correspondence of microelectrode mapping with magnetic resonance imaging for subthalamic nucleus procedures. Surg Neurol. 2005; 63(3):249–253. [PubMed: 15734516]
11. Tasker, RR.; Organ, LW.; Hawrylyshyn, PA. The thalamus and midbrain of man. Springfield: Charles C Thomas; 1982.
12. Finnis KW, Starreveld YP, Parrent AG, Sadikot AF, Peters TM. Three dimensional database of subcortical dlectrophysiology for dmage-guided stereotactic functional neurosurgery. IEEE Trans Med Imaging. 2003; 22(11):93–104. [PubMed: 12703763]

NIH-PA Author Manuscript

NIH-PA Author Manuscript

NIH-PA Author Manuscript

13. Finnis KW, Starreveld YP, Parrent AG, Sadikot AF, Peters TM. Application of a population based electrophysiological database to the planning and guidance of deep brain stereotactic neurosurgery. MICCAI. 2002
14. Nowinski WL, Belov D, Benabid AL. An algorithm for rapid calculation of a probabilistic functional atlas of subcortical structures from electrophysiological data collected during functional neurosurgery procedures. Neuroimage. 2003; 18:143–155. [PubMed: 12507451]
15. Nowinski WL, Belov D, Pollak P, Benabid AL. Statistical analysis of 168 bilateral subthalamic nucleus implantations by means of the probabilistic functional atlas. Neurosurgery. 2005; 57(4): 319–330. [PubMed: 16234681]
16. Nowinski WL. Towards construction of an ideal stereotactic brain atlas. Acta Neurochir (Wien). 2008; 150(1):1–13. discussion 13:14. [PubMed: 18030414]
17. Guo T, Finnis KW, Parrent AG, Peters TM. Development and application of functional databases for planning deep-brain neurosurgical procedures. Lecture notes in computer science (MICCAI). 2005; vol 3749:835–842.
18. Guo T, Finnis KW, Parrent AG, Peters TM. Visualization and navigation system development and application for stereotactic deep-brain neurosurgeries. Comput Aided Surg. 2006; 11(5):231–239. [PubMed: 17127648]
19. Toga AW, Thompson PM, Mori S, Amunts K, Zilles K. Towards multimodal atlases of the human brain. Nat Rev Neurosci. 2006; 7(12):952–966. [PubMed: 17115077]
20. Castro FJ, Pollo C, Cuisenaire O, Villemure J-G, Thiran J-P. Validation of experts versus atlas-based and automatic registration methods for subthalamic nucleus targeting on MRI. Int J Comput Assisted Radiol Surg. 2006; 1(1):5–12.
21. Castro FJ, Pollo C, Meuli R, Maeder P, Cuisenaire O, Cuadra MB, Villemure J-G, Thiran J-P. A cross validation study of deep brain stimulation targeting: from experts to atlas-based, segmentation-based and automatic registration algorithms. IEEE Trans Med Imaging. 2006; 25(11):1440–1450. [PubMed: 17117773]
22. D'Haese P-F, Cetinkaya E, Konrad PE, Kao C, Dawant BM. Computer-aided placement of deep brain stimulators: from planning to intraoperative guidance. IEEE Trans Med Imaging. 2005; 24(11):1469–1478. [PubMed: 16279083]
23. D'Haese P-F, Pallavaram S, Niermann K, Spooner J, Kao C, Konrad PE, Dawant BM. Automatic selection of DBS target points using multiple electrophysiological atlases. LNCS (MICCAI). 2005; 3750:427–434.
24. Dawant BM, D'Haese P-F, Pallavaram S, Li R, Yu H, Spooner J, Davis T, Kao C, Konrad PE. The VU-DBS project: integrated and computer-assisted planning, intra-operative placement, and post-operative programming of deep-brain stimulators. SPIE medical imaging 2007: visualization and image-guided procedures. 2007; vol 6509:650–907.
25. Pallavaram S, D'Haese P-F, Kao C, Yu H, Remple M, Neimat JS, Konrad PE, Dawant BM. A new method for creating electrophysiological maps for DBS surgery and their application to surgical guidance. Lecture notes in computer science (MICCAI). 2008; vol 5241(Part 1):670–677.
26. Guo T, Finnis KW, Deoni SCL, Parrent AG, Peters TM. Comparison of different targeting methods for subthalamic nucleus deep brain stimulation. Lecture notes in computer science (MICCAI). 2006; vol 4190:768–775.
27. Gerdes FU, Klein G, Nadjmi M, Schaltenbrand G. X-ray studies of the brain as a basis for stereotaxy (author's transl). J Neurol. 1975; 210:183–190. [PubMed: 51075]
28. Hariz MI, Bergenheim AT, Fodstad H. Air-ventriculography provokes an anterior displacement of the third ventricle during functional stereotactic procedures. Acta Neurochir (Wien). 1993; 123:147–152. [PubMed: 8237493]
29. Winkler D, Tittgemeyer M, Schwarz J, Preul C, Strecker K, Meixensberger J. The first evaluation of brain shift during functional neurosurgery by deformation field analysis. J Neurol Neurosurg Psychiatry. 2005; 76:1161–1163. [PubMed: 16024899]
30. Miyagi Y, Shima F, Sasaki T. Brain shift: an error factor during implantation of deep brain stimulation electrodes. Neurosurgery. 2007; 107:989–997.
31. Khan MF, Mewes K, Gross RE, Škrinjar O. Assessment of brain shift related to deep brain stimulation surgery. Stereotact Funct Neurosurg. 2008; 86:44–53. [PubMed: 17881888]

NIH-PA Author Manuscript

NIH-PA Author Manuscript

NIH-PA Author Manuscript

32. Halpern CH, Danish SF, Baltuch GH, Jaggi JL. Brain shift during deep brain stimulation surgery for Parkinson's disease. Stereotact Funct Neurosurg. 2008; 86:37–43. [PubMed: 17881887]
33. Fitzpatrick JM, Konrad PE, Nickele C, Cetinkaya E. Accuracy of customized miniature stereotactic platforms. Stereotact Funct Neurosurg. 2005; 83:25–31. [PubMed: 15821366]
34. Balachandran R, Mitchell JE, Dawant BM, Fitzpatrick JM. Accuracy evaluation of MicroTargeting™ platforms for deep-brain stimulation using virtual targets. IEEE Trans Biomed Eng. 2009; 56(1):37–44. [PubMed: 19224717]
35. D'Haese, P-F.; Pallavaram, S.; Yu, H.; Spooner, J.; Konrad, PE.; Dawant, BM. Lecture notes in computer science (WBIR). Vol. vol 4057. The Netherlands: Utrecht; 2006. Deformable physiological atlas-based programming of deep brain stimulators: a feasibility study; p. 144-150.
36. Rohde GK, Aldroubi A, Dawant BM. The adaptive bases algorithm for intensity-based nonrigid image registration. IEEE Trans Med Imaging. 2003; 22(11):1470–1479. [PubMed: 14606680]
37. Maes F, Collignon A, Suetens P. Multimodality image registration by maximization of mutual information. IEEE Trans Med Imaging. 1997; 16(2):187–198. [PubMed: 9101328]
38. Wells WM, Viola P, Atsumi H, Nakajima S, Kikinis R. Multi-modal volume registration by maximization of mutual information. Med Image Anal. 1996; 1(1):35–52. [PubMed: 9873920]
39. Pluim JP, Maintz JB, Viergever MA. Mutual-information-based registration of medical images: a survey. IEEE Trans Med Imaging. 2003; 22(8):986–1004. [PubMed: 12906253]
40. Rosenbaum, BP.; D'Haese, P-F.; Yu, H.; Pallavaram, S.; Dawant, BM.; Neimat, JS.; Konrad, PE. Brain shift during deep brain stimulation surgery correlates directly to pneumocephalus and inversely to age. American Society of Sterotactic and Functional Neurosurgery (ASSFN) Biennial meeting; Vancouver, BC, Canada. 2008.
41. Butson CR, McIntyre CC. Current steering to control the volume of tissue activated during deep brain stimulation. Brain Stimul. 2008; 1(1):7–15. [PubMed: 19142235]
42. Pallavaram S, Dawant BM, Koyama T, Yu H, Neimat JS, Konrad PE, D'Haese P-F. Validation of a fully automatic method for the routine selection of the anterior and posterior commissures in MR images. J Stereotact Funct Neurosurg. 2009; 87:148–154.
43. The Deep Brain Stimulation for Parkinson's disease study group. Deep-brain stimulation of the subthalamic nucleus or the pars interna of the globus pallidus in Parkinson's disease. N Engl J Med. 2001; 345:956–963. [PubMed: 11575287]

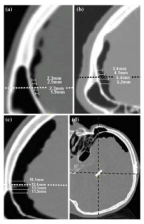

Fig. 1.

Frontal portion of a sagittal slice (after a 90° rotation for easy visualization) on post-operative CT for patients in **a** low, **b** medium, **c** large shift groups showing air pocket. Width of the air pocket is measured from the inner table of the calvarium at the lead level as shown. Sample measurements in mm are shown. **d** Typical head orientation in the scanner with the patient lying supine. The *dashed horizontal line* in **a**, **b** and **c** is a vector passing through the implant in the direction of gravity

NIH-PA Author Manuscript NIH-PA Author Manuscript NIH-PA Author Manuscript

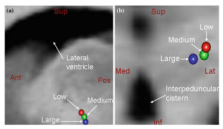

Fig. 2.

Centroids of somatotopy clusters of low (*red*), medium (*blue*) and large (*green*) brain shift patients overlaid on the atlas MRI. **a** Sagittal view showing a lateral ventricle and **b** coronal view showing the interpeduncular cistern for reference

NIH-PA Author Manuscript
NIH-PA Author Manuscript
NIH-PA Author Manuscript

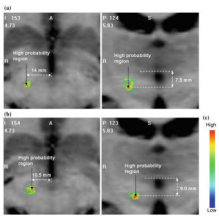

Fig. 3.
Axial and coronal slices of the eye deviation maps containing the high probability points for **a** low brain shift, **b** medium-large brain shift groups overlaid on the atlas MRI, **c** color scale

NIH-PA Author Manuscript NIH-PA Author Manuscript NIH-PA Author Manuscript

NIH-PA Author Manuscript
NIH-PA Author Manuscript
NIH-PA Author Manuscript

Table 1

Locations of centroids and medians of the somatotopy clusters in AC–PC coordinates for the low, medium and large shift groups

	(a) Cluster centroids			(b) Cluster medians		
	Low	**Medium**	**Large**	**Low**	**Medium**	**Large**
Posterior (mm)	1.94	2.90	3.06	1.96	2.82	2.51
Lateral (mm)	13.92	13.57	11.27	13.39	13.28	11.73
Inferior (mm)	3.20	4.53	5.36	2.75	4.59	5.62